Potentiated Electron Transference in α-Ag 2 WO 4 Microcrystals with Ag Nanofilaments as Microbial Agent

ARTICLE *in* THE JOURNAL OF PHYSICAL CHEMISTRY A · FEBRUARY 2014

Impact Factor: 2.69 · DOI: 10.1021/jp410564p · Source: PubMed

THE JOURNAL OF PHYSICAL CHEMISTRY A

Article

pubs.acs.org/JPCA

Potentiated Electron Transference in α-Ag_2WO_4 Microcrystals with Ag Nanofilaments as Microbial Agent

Valéria M. Longo,*[,†] Camila C. De Foggi,[‡] Mateus M. Ferrer,[§] Amanda F. Gouveia,[§] Rafaela S. André,[§] Waldir Avansi,[§] Carlos E. Vergani,[‡] Ana L Machado,[‡] Juan Andrés,[∥] Laécio S. Cavalcante,[⊥] Antonio C. Hernandes,[†] and Elson Longo[¶]

[†]INCTMN-USP, Universidade de São Paulo, Instituto de Física de São Carlos, 13560-970 São Carlos, SP, Brazil

[‡]Department of Dental Materials and Prosthodontics, UNESP − Univ. Estadual Paulista, P.O. Box 355, 14801-903 Araraquara, SP, Brazil

[§]INCTMN-UFSCar, Universidade Federal de São Carlos, P.O. Box 676, 13565-905 São Carlos, SP, Brazil

[∥]Department of Química-Física-Analítica, Universitat Juame I, 12071 Castello, Spain

[⊥]CCN-DQ-GERATEC, Universidade Estadual do Piauí, P.O. Box 381, 64002-150 Teresina, PI, Brazil

[¶]INCTMN-UNESP, Universidade Estadual Paulista, P.O. Box 355, CEP 14801-907 Araraquara, SP, Brazil

Supporting Information

ABSTRACT: This study is a framework proposal for understanding the antimicrobacterial effect of both α-Ag_2WO_4 microcrystals (AWO) synthesized using a microwave hydrothermal (MH) method and α-Ag_2WO_4 microcrystals with Ag metallic nanofilaments (AWO:Ag) obtained by irradiation employing an electron beam to combat against planktonic cells of methicillin-resistant *Staphylococcus aureus* (MRSA). These samples were characterized by X-ray diffraction (XRD), FT-Raman spectroscopy, ultraviolet visible (UV−vis) measurements, field emission scanning electron microscopy (FE-SEM), transmission electron microscopy (TEM), and high resolution transmission electron microscopy (HRTEM). The results reveal that both AWO and AWO:Ag solutions have bacteriostatic and bactericidal effects, but the irradiated sample is more efficient; i.e., a 4-fold of the MRSA planktonic cells as compared to the nonirradiated sample was observed. In addition, first principles calculations were performed to obtain structural and electronic properties of AWO and metallic Ag, which provides strong quantitative support for an antimicrobacterial mechanism based on the enhancement of electron transfer processes between α-Ag_2WO_4 and Ag nanoparticles.

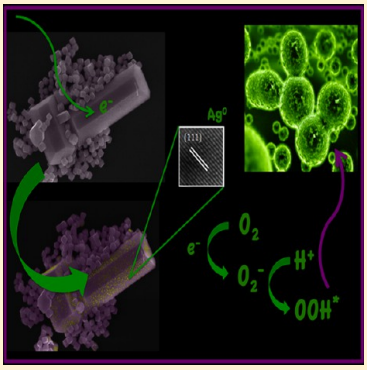

1. INTRODUCTION

Among the various types of potential functional materials, tungsten-based oxides are an important class of materials that exhibit various functional properties that depend on the structure.[1] In the last decades these materials were extensively studied because of their excellent optical properties for technological applications. In particular, Ag_2WO_4 belongs to the oxoargentates family,[2] and it is an inorganic material containing a rich variety of polymorphs: α-orthorhombic (α-Ag_2WO_4) with a space group of *Pn*2*n*, β-hexagonal with a space group of *P*63/*m*, and γ-cubic with a space group of *Fd*3*m* depending on the acid or alkaline pH range.[3,4]

The orthorhombic structure of α-Ag_2WO_4 exhibits a complex network composed of [WO_6] and [AgO_y] (y = 7, 6, 4, and 2) moieties as constituent clusters of this material whose internal vibration spectra provide information on the structure and order−disorder effects in crystal lattices.[5,6] This structural pattern is a key characteristic for a complete understanding of α-Ag_2WO_4 potentialities.

In this framework, the structural order−disorder in the lattice dictates physical and chemical properties of materials and is strongly correlated with structural factors such as the cluster arrangement, and thus materials can be described in terms of the constituent cluster packing of atoms that can be considered as structural motifs.[7] Breaking symmetry processes of these clusters such as distortions, breathings, and tilts create a huge number of different structures; this phenomenon can be related to short-, intermediate- and long-range structural order−disorder that subsequently creates different materials properties. Therefore, for a α-Ag_2WO_4 material, structural and electronic properties can primarily be associated with cluster constituents, and the disparity or mismatch of both clusters can induce structural order−disorder effects that will significantly influence their

Special Issue: Energetics and Dynamics of Molecules, Solids, and Surfaces - QUITEL 2012

Received: October 25, 2013
Revised: February 17, 2014

   dx.doi.org/10.1021/jp410564p | *J. Phys. Chem. A* XXXX, XXX, XXX−XXX

luminescence and photodegradation processes. These processes are important in novel functional nanomaterials; therefore, in recent decades, understanding fundamental mechanisms underlying these processes has been a major goal of experimental and theoretical research in chemical physics and physical chemistry.[8]

In the last few decades, hospital infection cases have rapidly increased; most of them are related to methicillin-resistant *Staphylococcus aureus* (MRSA) bacteria.[9] Bacteremia caused by MRSA is associated with increased mortality rates[10] and has been identified more frequently in elderly or immunocompromised patients.[11] Multiple factors influence outcomes for MRSA bacteremia patients, and the most consistent predictor of mortality is age with older patients being twice as likely to die.[12] There are now limited therapeutic options for treating serious bacterial infections, and in the face of increasing resistance, there is an urgent need for new antibiotics. In particular, vancomycin hydrochloride has been the accepted standard of therapy for MRSA infections.[13] However, it is becoming less than optimal for treating MRSA and other resistant gram-positive bacteria. Vancomycin treatment failures for MRSA infections have increasingly been reported in the literature despite apparent in vitro susceptibility, particularly for strains with a minimum inhibitory concentration (MIC) of 2 μg/mL.[14] Reported data strongly suggest that patients with MRSA bloodstream infections with vancomycin MICs of $\geq$1.5 μg/mL respond poorly to vancomycin. Thus, optimal treatment strategies to prevent the mortality associated with reduced vancomycin susceptibility in *S. aureus* bacteremia worldwide is a crucial research world subject to be solved.

Surfaces with antimicrobacterial properties are highly desired in applications that require a protective barrier against infection. In this context, nanoparticles have been investigated as an alternative to traditional antibiotics due their unique chemical and physical properties. Due to epidemics caused by different pathogenics that target multiple cellular pathways, a research field devoted to the developing new classes of powerful antibacterial agents is imperative.[15−17]

In several applications, noble nanoparticles (Ag, Au, Pt) deposited on a semiconductor surface to form a metal−semiconductor composite have been proposed as promising materials because of their advantageous features related to a surface plasmon resonance effect, additional active sites and/or an electronic trap.[18]

Due to their potent antibacterial activity, silver nanoparticles (AgNPs) have gained acceptance in a wide array of applications in consumer products such as textiles, personal care products, cosmetics, and medical.[19] In addition, recent research has been devoted to AgNPs and their uses in medicine[20−23] A wide spectrum of studies confirmed that AgNPs possess excellent antimicrobacterial activity to combat a broad spectrum of microbes,[15,17,24−30] and they are effective against a wide range of organisms (e.g., bacteria, algae, zooplankton, and fish)[31−34] and for gram-negative and gram-positive bacteria.[29,35−37] AgNPs have also been reported to reduce microbial infection in skin and burn wounds and to prevent bacterial colonization on various devices surfaces such as catheters and implants.[38−42]

Compared with conventional antimicrobacterial molecules, AgNPs with the advantage of large surface areas bind efficiently to microorganisms and provide enhanced antimicrobial action,[17,43,44] and AgNPS, alone or supported on a ceramic support, are used as antimicrobial fillers in textiles[45] and polymers[46] for food-packaging[47] and biomedical applications,[48,49] for antimicrobial paints,[50] and potentially for drug delivery.[51] In addition, AgNPS are less toxic to human cells as compared to other metals.[52] Possible targets for silver inside the microbial cells are numerous and hence the development/evolution of its resistance to silver compounds is limited.[26,53] As a general trend, it has been assumed that AgNPs attach to the negatively charged surface of the cell membrane, which causes protein denaturation and subsequent cell death.[54] On the other hand, Panacek et al.[29] proposed that these nanoparticles can penetrate inside the bacteria and cause cell damage by interaction with sulfur and phosphorus compounds such as proteins and DNA.

Although gram-positive bacteria such as MRSA have no outer membrane, they are enclosed within a thick peptidoglycan layer (15−80 nm),[22,55] which is a polymer consisting of sugars and amino acids that forms a mesh-like cell wall on the outside of the plasma membrane. This rigid layer of peptidoglycan is harder to penetrate and offers only a limited number of anchoring sites for AgNPs, which facilitates a more difficult attack.[56] Kim et al.,[16] reported that the gram-positive bacteria *S. aureus* was less susceptible to AgNPs than gram-negative *Escherichia coli*. Thus, these properties make AgNPs a good candidate for overcoming antibiotic resistant bacteria; however, a global view of their functioning is still missing.

Very recently, our group reported[57] the synthesis of hexagonal rod-like elongated α-Ag_2WO_4 nanocrystals by sonochemistry, coprecipitation, and conventional hydrothermal methods. It was discovered that the α-Ag_2WO_4 crystal lattice contains several distortions on [AgO_7], [AgO_6], [AgO_4], and [AgO_2] clusters through different bond angles within O−Ag−O in the crystal lattice. We also reported[58] the fascinating real-time in situ electron-driven silver filament growth process from the unstable α-Ag_2WO_4 crystals matrix using field emission scanning electron microcopy (FE-SEM) and electron irradiation by transmission electron microscopy (TEM). High-resolution TEM (HRTEM) images indicate that these metallic Ag filaments grow on α-Ag_2WO_4 crystal surfaces. More recently, a combined experimental and theoretical study was conducted on the structure and electronic properties of α-Ag_2WO_4 to clarify the photoluminescence processes of Ag filaments on α-Ag_2WO_4 crystals.[59] The present work can be considered as a natural prolongation of previous studies, in which the microbial property of this exciting material is emphasized.

Studies involving interfaces between Ag and α-Ag_2WO_4 are crucial to evaluate the improvement in formed nanocomposite properties. Using a microwave hydrothermal (MH) method, we synthesized α-Ag_2WO_4 (AWO) and herein we demonstrate that metallic AgNPs formed by electron beam irradiation on α-Ag_2WO_4 microcrystal surfaces (AWO:Ag) produce a remarkable antibacterial effect on planktonic cells of *S. aureus*. Because of the importance of this problem and the paucity of quantitative experimental results, the goal of our study is to determine this antimicrobacterial effect. Therefore, both AWO and AWO:Ag samples were characterized by X-ray diffraction (XRD), FT-Raman spectroscopy, ultraviolet−visible (UV−vis) measurements, and electron microscopy where an electron beam is used for structural and morphological characterization. Due to difficulties in assigning correct electronic responses at an atomistic resolution, first-principles calculations were employed to evaluate the electronic structure of α-Ag_2WO_4 and metallic Ag to rationalize experimental results; thus we propose a model to explain the antimicrobacterial mechanism. Generated electrons and holes at the solid surface under electron irradiation were

dx.doi.org/10.1021/jp410564p | J. Phys. Chem. A XXXX, XXX, XXX−XXX

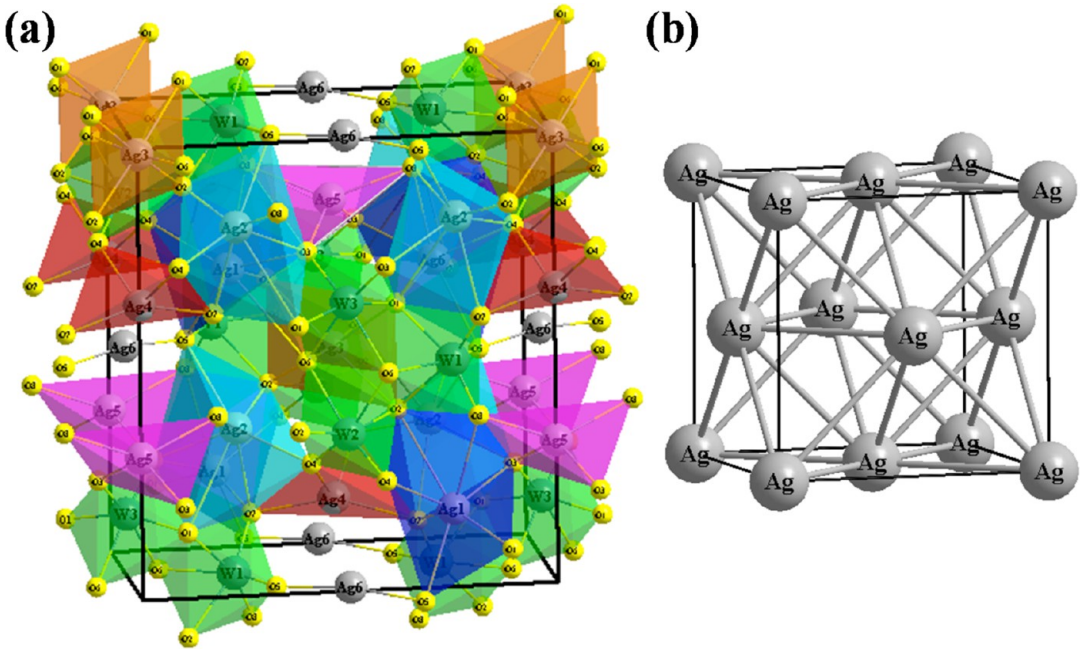

Figure 1. Bulk structures: (a) orthorhombic α-Ag_2WO_4; (b) cubic metallic Ag.

therefore investigated using a methodology already illustrated in our previous research.[57]

2. MATERIALS AND METHODS

2.1. Preparation of the Samples. α-Ag_2WO_4 crystals were prepared at 120 °C for 1 h with 1 g of polyvinylpyrrolidone (PVP) with a formula $(C_6H_9NO)_n$, where n = 29−32, with an average molecular weight of 40 000 and a 99% purity (Sigma-Aldrich) by the MH method. A typical α-Ag_2WO_4 crystal synthesis procedure is described as follows: 1×10^{-3} mol of tungstate sodium dihydrate ($Na_2WO_4{\cdot}2H_2O$; 99.5% purity, Sigma-Aldrich) and 2×10^{-3} mol of silver nitrate ($AgNO_3$; 99.8% purity, Sigma-Aldrich) were separately dissolved with deionized water contained in two 50 mL plastic tubes (Falcon). Before the salt dissolution was started, 0.5 g of anionic surfactant PVP was dissolved in both tubes. In the sequence, 100 mL of this resulting suspension was transferred into a Teflon autoclave vessel without stirring. Then the Teflon reactor was sealed and placed inside an adapted domestic microwave system and processed at 120 °C for 1 h. The temperature of the system was monitored using an in-vessel temperature sensor (Model CNT-120, INCON Electronic Ltd. from São Carlos-SP, Brazil). MH reactions were carried out in 150 mL polyethylene vessels. The α-Ag_2WO_4 crystal was obtained as a light beige finely powdered precipitate. The resulting suspension was washed with deionized water and acetone several times to remove any remaining Na^+ ions and organic compounds. Finally, this light beige powdered precipitate was collected and dried with acetone at room temperature for 6 h.

The growth of metallic Ag nanofilaments in α-Ag_2WO_4 crystals was performed in a scanning electron microscope (SEM) model 30 kV (Zeiss DSM 940A) operating at 30 kV for 30 min.

2.2. Characterization of Samples. The α-Ag_2WO_4 crystal and α-Ag_2WO_4 with Ag nanorods particles were structurally characterized by XRD patterns using a D/Max-2500PC diffractometer (Rigaku, Japan) with Cu Kα radiation (λ = 1.5406 Å) in the 2θ range from 10° to 70° in the normal routine with a 2°/min scanning velocity and 0.02° step. Micro-Raman measurements were recorded using the LabRAM HR 800 mm model (Horiba; Jobin-Yvon, France). High-resolution Raman spectra were taken with a He−Ne laser at 632.81 nm (model CCD DU420AOE325) operating at 25−1000 cm^{-1}, with a maximum output power maintained at 6 mW. A 50 μm lens was used to prevent sample overheating. UV−vis spectra were taken using a Varian spectrophotometer (Cary 5G model) in a diffuse-reflectance mode.

The α-Ag_2WO_4 microcrystals shapes and sizes were observed using FE-SEM Inspect F50 model (FEI Company, Hillsboro, OR) operated at 15 kV when the electron beam reached the sample, and the focus was adjusted (time zero). α-Ag_2WO_4 microcrystals with Ag nanofilaments were observed by FE-SEM in the same conditions described previously, but 30 min after the focus was adjusted. A TEM analysis was performed using JEM 2100F TEM/STEM microscope operating at 200 kV. Chemical sample analyses were performed by energy dispersive X-ray spectroscopy (EDS) using an EDS Thermo-Noran equipped with a Si detector attached to the JEM 2100F. Specimens for TEM images were obtained by drying droplets of as-prepared samples from an acetone dispersion that had been sonicated for 10 min and deposited on 300 mesh Cu grids.

2.3. Antimicrobacterial Activity Analysis. To determine the antimicrobacterial effect of synthesized AWO and AWO:Ag samples, using a broth microdilution assay, MIC and minimum bacterial concentrations (MCB) to planktonic cells were determined as described by Clinical and Laboratory Standards Institute (CLSI) (document M7-A7, 2006) with modifications. A standard strain of methicillin-resistant *S. aureus* (MRSA) from the American Type Culture Collection (ATCC 33591) was used. To prepare the inoculum, MRSA was streaked onto mannitol salt agar (MSA, Acumedia Manufactures Inc. Baltimore, Maryland, USA) and incubated at 37 °C for 48 h. One loopful of this culture was transferred to 10 mL of tryptic soy broth medium (TSB, Acumedia Manufactures, Inc. Baltimore, Maryland, USA) and incubated in an orbital shaker overnight at 37 °C and 75 rpm. Then MRSA cells were harvested by centrifugation at 5000 rpm

dx.doi.org/10.1021/jp410564p | J. Phys. Chem. A XXXX, XXX, XXX−XXX

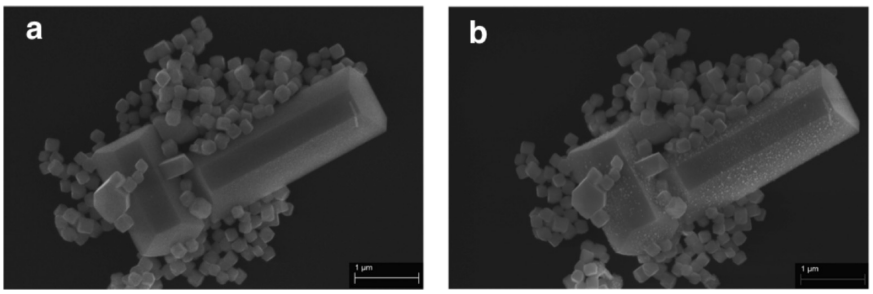

Figure 2. FE-SEM images of α-Ag_2WO_4 crystal morphology (a) before (AWO; time zero) and (b) after 30 min of Ag filaments growth stimulated by the electron beam on the α-Ag_2WO_4 surface (AWO:Ag) obtained in a high vacuum.

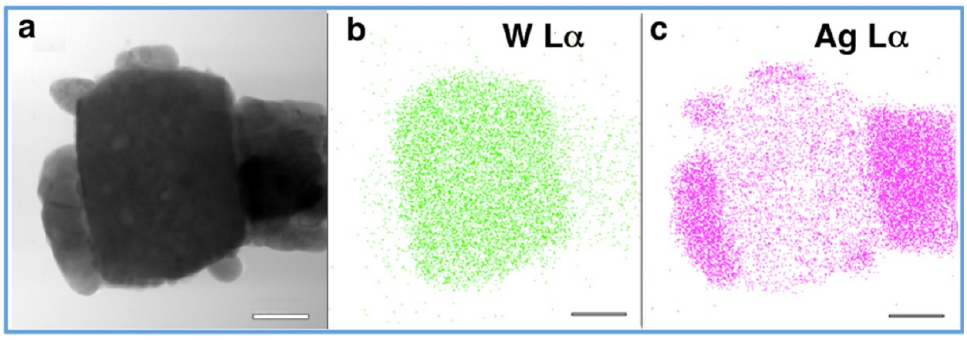

Figure 3. (a) Bright field STEM image of an isolated particle. (b) and (c) EDS mapping of W Lα and Ag Lα, respectively. (Scale bar = 50 nm in a, b, and c.)

for 5 min, washed twice with phosphate-buffered saline (PBS) (pH 7.2), and resuspended in TSB medium.

MIC and MBC were determined by incubating MRSA on a 96-well microtiter plate for 24 h at 37 °C and exposed to serial 2-fold dilution in a TSB medium of the α-Ag_2WO_4 solution (from 1000 to 1.95 μg/mL). An inoculated TSB medium without the α-Ag_2WO_4 solution was used as a positive control; an uninoculated TSB medium was used as a negative control. For AWO and AWO:Ag samples, the MIC was defined as the lowest concentration where there was no visible growth by visual inspection. To establish the MBC, aliquots from each well were removed and inoculated (10 μL) on plates (in duplicate). After 48 h of incubation at 37 °C, the colony-forming units per milliliter (CFU/mL) were calculated and log 10 transformed. The MBC value was defined as the lowest concentration of the AWO and AWO:Ag solutions resulting in no growth. All experiments were performed in triplicate on three independent occasions.

3. COMPUTATIONAL METHOD AND MODELS

The simulation was performed using a periodic approximation as implemented in the CRYSTAL09 computer code.[60] The computational method is based on density functional theory (DFT) in conjunction with Becke's three-parameter hybrid nonlocal exchange functional[61] combined with the Lee–Yang–Parr gradient-corrected correlation functional, B3LYP.[62] The hybrid density-functional method has been extensively used for molecules and provides an accurate description of crystalline structures, bond lengths, binding energies, and band gap values.[63] The diagonalization of the Fock matrix was performed at adequate *k*-point grids (Pack–Monkhorst 1976) in the reciprocal space.[64] Thresholds controlling the accuracy of the calculation of the Coulomb and exchange integrals were set to 10^{-8} (ITOL1 to ITOL4) and 10^{-14} (ITOL5), and the percent of Fock/Kohn–Sham matrix mixing was set to 30 (IPMIX 1/4 30). The dynamic matrix was computed by the numerical evaluation of the first derivative of the analytical atomic gradient. The system point group symmetry was fully exploited to reduce the number of points considered. For each numerical step, the residual symmetry was preserved during the self-consistent field (SCF) and gradient calculations. Atomic centers for Ag and W atoms have been described by basis sets (PS-11d3G pseudopotential basis sets) provided by the CRYSTAL basis set library, and the O atoms have been described by the standard 6-31G*.[65] *k*-point sampling was chosen as 36 points within the irreducible part of the Brillouin zone. The XcrysDen program was used to design band structure diagrams.[66]

Figure 1a,b illustrates the two models built to simulate the α-Ag_2WO_4 orthorhombic bulk crystal and cubic Ag-metallic structures.

4. RESULTS AND DISCUSSION

Figure 2 shows FE-SEM images of as-obtained samples before (time considered equal to zero) and after the growth of Ag filaments stimulated by electron beam irradiation on the α-Ag_2WO_4 surface, which were obtained in high vacuum (1×10^{-5} Pa).

α-Ag_2WO_4 microcrystals have a hexagonal rod-like elongated, cubic-like, and triangular-like shapes that are acquired after a rapid approach and a focus adjustment (time zero) (Figure 2a). Figure 2b shows the α-Ag_2WO_4 morphology and its surface after 30 min of electron beam exposition where the growth of nanoparticles on the α-Ag_2WO_4 crystal surface is visible. According to our previous reasearch a reasonable amount of electrons induces the continuous axial flow of metallic Ag particles.[58] FE-SEM analyses revealed that this axial Ag growth process is highly reproducible.

dx.doi.org/10.1021/jp410564p | J. Phys. Chem. A XXXX, XXX, XXX–XXX

Exposure to the energetic TEM electron beam can modify amorphous or nanocrystalline structures of solid materials. Very recently, using the chemical reduction method, Tsuji et al.[67] monitored the rapid transformation of various Ag nanostructures from Ag^+ ions to Ag^0 in solution by time-dependent surface plasmon resonance. In another example, using in situ TEM images, Yasuda et al.[68] reported the indium oxide reduction process at 820 °C in metallic indium and intermetallic species ($PdIn_3$).

To check the chemical composition of the as-obtained α-Ag_2WO_4 with metallic Ag^0, an elemental X-ray mapping was performed on a single particle. Figure 3a shows a bright field scanning transmission electron microscopy (STEM) image of a single nanostructure where the elemental X-ray mappings were performed. The EDS results (Figure 3b,c) confirm that electron-driven structures formed after electron exposure are composed mainly of Ag elements whereas the "pristine" nanoparticle (cube) mainly contains W elements with a smaller quantity Ag as expected.[58]

HRTEM analyses of the Ag filament on the α-Ag_2WO_4 sample after electron irradiation using a TEM microscope also were performed. In Figure 4, an expanded view of the region is depicted and analysis results reveal that the lattice parameter is about 2.3 Å, which is consistent with the (111) plane of the cubic structure of the Ag metallic nanofilament. HRTEM and EDS results confirm the growth of Ag metallic nanofilaments from a α-Ag_2WO_4 crystal when exposed to an electron beam.

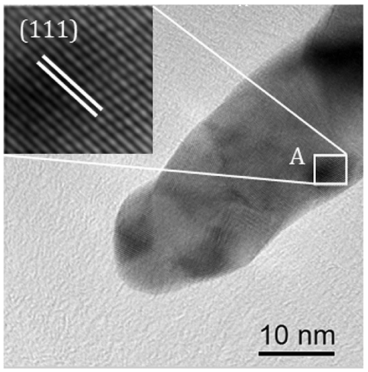

Figure 4. HRTEM analyses of the Ag filament on a α-Ag_2WO_4 sample. Inset: an expanded view of region A.

The α-Ag_2WO_4 crystal lattice contains different $[WO_6]$, $[AgO_7]$, $[AgO_6]$, $[AgO_4]$, and $[AgO_2]$ clusters, as discussed before. Thus the electron excess provoked by electron irradiation induces electronic and structural modifications on the unstable α-Ag_2WO_4 crystals and forms metallic Ag nanofilamentss.[58] This process generates complex vacancies of V'_{Ag} and V^x_O (where V^x_O = V^x_O, $V^{\bullet}_O$, $V^{\bullet\bullet}_O$). An important component of the α-Ag_2WO_4 crystal matrix and Ag nanofilaments growth is the nonexistence of an interface between them (Figure 3b,c). This feature attributes special and unique properties of this new material, which are not a core−shell, a decorated structure, or even a heterostructure, and is therefore a continuous structure composed of a semiconductor and a metal.

XRD patterns (Supporting Information, Figure 1SI) indicate that both AWO and AWO:Ag have an orthorhombic structure with a space group of *Pn2n*.[4] These crystals have sharp and well-defined diffraction peaks, which indicates a structural order and crystallinity at the lattice long-range without any deleterious phases. However, it is difficult to identify any conclusions concerning the existence of Ag nanoparticles on the lattice in these crystals from XRD measurements.[69] Moreover, all diffraction peaks are in good agreement with the respective Inorganic Crystal Structure Data (ICSD) base No. 4165.

Vibrational Raman modes characteristic of the oxoargentate phase in the octahedral structure were observed for the two samples having point-group symmetry C^{10}_{2v} at room temperature (Figure 5). The lower translational active-mode of A_{1g} (57 cm^{-1}) corresponds to external or lattice phonons associated with the Ag heavy cation motion in the rigid molecular unit. Internal vibrations are associated with movements inside the $[WO_6]$ molecular group, which reveal several peaks correspond with Raman-active internal modes of distorted octahedra $[WO_6]$ clusters: A_1, B_1, A_2, and B_2. Figure 5b confirms good agreement between observed vibrations and the literature.[70] However, fifteen actives Raman modes were noted, which is two less than the modes detected by Turkovic et al.,[70] which can probably be explained by a low Raman signal. Small shifts in observed Raman mode positions can arise from different factors such as

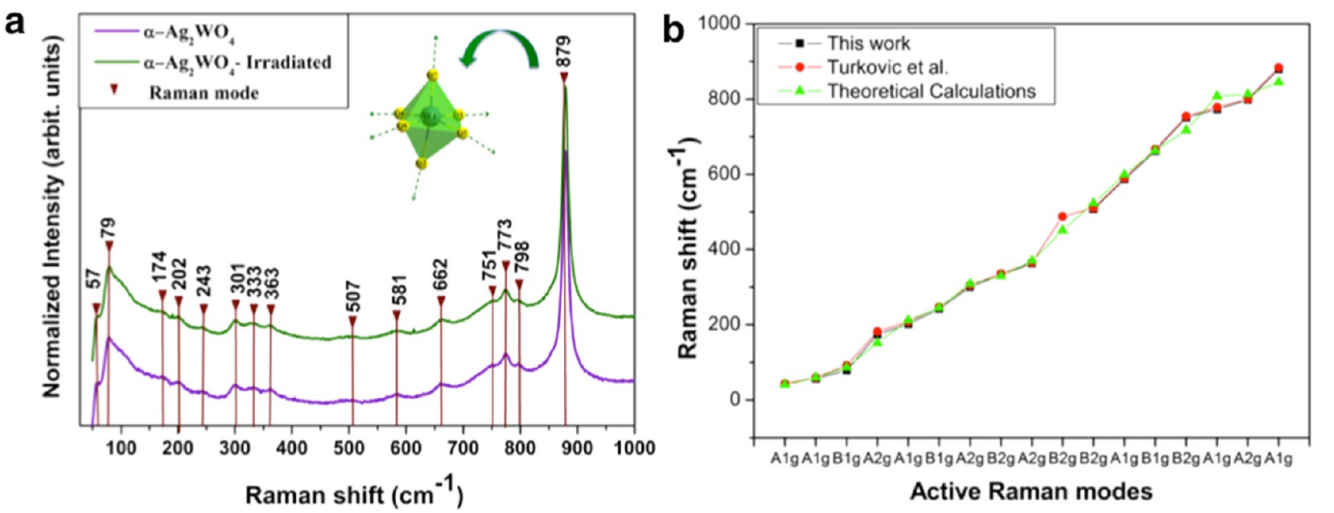

Figure 5. (a) Actives Raman modes for an orthorhombic α-Ag_2WO_4 crystal structure at room temperature, and (b) theoretical active Raman modes and comparison with experimental results of this work and tresults reported by Turkovic et al.[70]

dx.doi.org/10.1021/jp410564p | J. Phys. Chem. A XXXX, XXX, XXX−XXX

preparation methods, average crystal size, interaction forces between the ions, or the degree of structural order in the lattice.[71] More specifically, α-Ag_2WO_4 crystals prepared by the MH method possess a well-defined Raman-active vibration mode related to symmetric stretching vibrations from (←O←W→O→) bonds of octahedral [WO_6] clusters assigned by the 879 cm^{-1} Raman mode.

Moreover, active Raman modes confirm that α-Ag_2WO_4 is structurally ordered at short-range, but the peaks are relatively wide, which is an indication of structural disorder at this level. However, X-ray absorption near edge structure (XANES) and extended X-ray absorption fine structure (EXAFS) analyses also confirm this structural feature.[57]

Note that Raman analysis is incapable of detecting any significant change in both AWO and AWO:Ag samples. In contrast, results obtained from the FEG-SEM image and TEM analysis reveal a surface differentiation between the samples. Raman spectroscopy is a powerful tool to distinguish surface changes in nanomaterials, but as the crystal grows, these changes are weak and therefore the formation of a metallic Ag cubic phase is not detected by this technique because Raman technique is an intrinsic bulk analysis.

The AWO sample has one well-defined absorption front whereas the irradiated crystals typically exhibit a continuous smooth absorption increase as a function of the energy, which suggests localized states inside the band gap (Supporting Information, Figure 2SI). Optical gaps obtained by extrapolation of the linear curve regions according to the Wood and Tauc method[72] are 3.1 eV for the nonirradiated sample and 2.4 eV for the irradiated sample. The drastic reduction in the band gap of irradiated sample can occurs by a plasmonic effect of Ag nanorods in surface, by the presence of this new structure on the surface creating new localized levels in the band gap or most probably by both effects. AWO and AWO:Ag have a local far-field interaction in the band gap, which probably facilitates hybridization between α-Ag_2WO_4 and Ag metallic band gaps and results in a total reduction of 0.7 eV for the total band gap. In addition, the continuously increasing smooth absorption front as a function of the energy is linked to localized electronic levels in the band gap which is introduced by de Ag metallic nanofilaments effects on the surface.

Figure 6 shows total and partial DOS projected on the 4d, 5d, and 2p orbitals of Ag, W, and O atoms, respectively, for neutral α-Ag_2WO_4 and the Ag cubic structure. For the neutral α-Ag_2WO_4, the projected DOS on the W atom is basically determined by 5d orbitals in the conduction band (CB) and the $5d_{z^2}$ orbitals. The valence band (VB) is primarily derived from hybridized O 2p and Ag 4d orbitals, whereas the metallic Ag has a Fermi energy of −3.17 eV with a conductor electronic structure character and free electrons forming continuous electronic states.

Theoretical calculations are in concordance with UV−vis spectra experimental results. New levels observed in the α-Ag_2WO_4 irradiated structure are derived from the disordered semiconductor surface after Ag metallic growth and from metallic Ag that emerged from the surface which reduced the total band gap (Supporting Information Figure 2SI).

An analysis of the results shown in Figure 7 reveals that MRSA was inactivated and killed by α-Ag_2WO_4 solutions and that this effect was concentration-dependent. The planktonic MIC/MBC value for the solution irradiated by an electron beam from the electronic microscope was considerably lower (31 μg/mL) than the nonirradiated value (125 μg/mL). Although both α-Ag_2WO_4 solutions had bacteriostatic and bactericidal effects to combat the

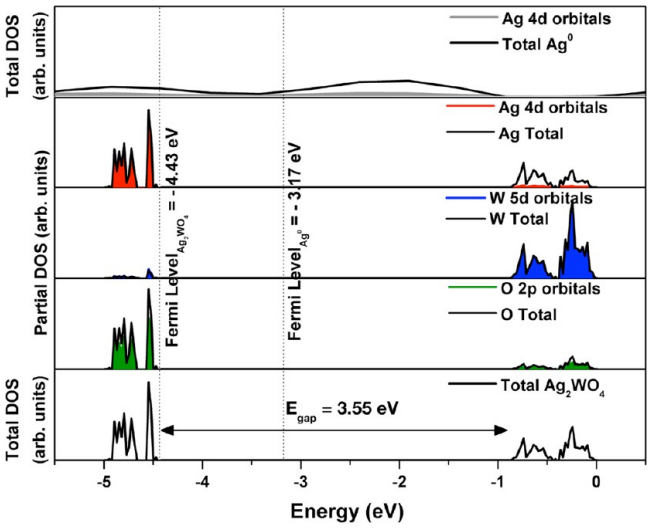

Figure 6. Total and partial DOS projected on 4d, 5d, and 2p orbitals of Ag, W, and O atoms, respectively, for neutral α-Ag_2WO_4 and Ag^0 cubic structures.

microorganism tested, a 4-fold reduction in MIC/MBC was observed for MRSA in sample II.

Note that α-Ag_2WO_4\Ag junction properties are related to surface plasmons on AgNPs, which generates exceptionally high localized electromagnetic fields. This increased activity of AWO:Ag can be due to the interaction with the disorder surface from semiconductor and Ag nanofilaments (more oxidant) in the surface and the microbial cell surface. The α-Ag_2WO_4 attachment with Ag nanofilaments to the plasma membrane may change its permeability by altering the adenosine triphosphate pool and the proton motive force.[15,24] Once they are into the cells, silver ions released from AgNPs can interact with phosphorus moieties in DNA and result in DNA replication inactivation; silver ions or can also react with sulfur- and phosphorus-containing proteins, which inhibits enzyme functions.[73] Interaction of AgNPs with the DNA has clearly been observed in an TEM analysis that results in a densely packed condensed DNA that loses its ability to replicate.[74] There are other known pathways for the interactions between AgNPs and bacteria[22] such as (i) interference in the mitochondrial respiratory chain, which reduces dehydrogenase activity,[74,75] and (ii) production of reactive oxygen species (mainly superoxide radical anion),[16,31,55] which may also target lipids, DNA, RNA, and proteins and cause severe consequences to the cell functions.[76]

Many of these observations can be understood in terms of surface plasmons when the modifications to the electronic structure induced by the AgNPs are considered as the collective oscillations of CB electrons following electric field vector variations of the incident beam.[77,78] Thus plasmon excitation provides an ultrafast method for delivering energy to the immediate vicinity of AgNPs, and this energy is employed to promote electron transfer processes.[79] As a consequence, the Ag plasmon band should be displaced upon subtracting electrons to the overall α-Ag_2WO_4 semiconductor variation.

On the basis of both experimental and theoretical results, we propose a model where the driving force of this dynamic process is the order−disordered effect at short-range between the α-Ag_2WO_4 and metallic Ag. In terms of the electronic structure, the VB and CB of α-Ag_2WO_4 are positioned (energetically) between the Fermi energy of Ag. Therefore, the activated α-Ag_2WO_4 semiconductor can act as a sink of generated electrons that can

dx.doi.org/10.1021/jp410564p | J. Phys. Chem. A XXXX, XXX, XXX−XXX

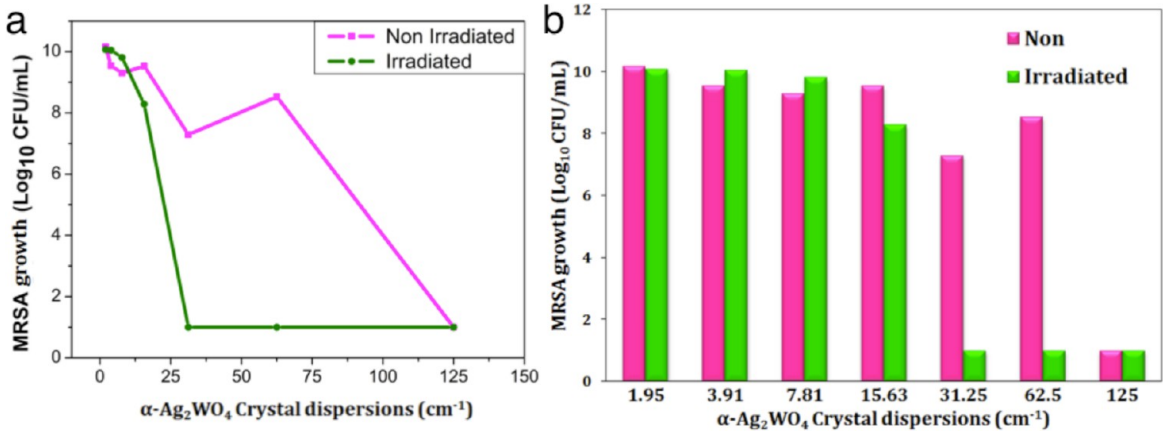

Figure 7. MRSA growth as a function of different concentrations of α-Ag_2WO_4 nanofilaments solutions.

serve as a reservoir for photoinduced charge and Ag acts as charge carriers and extends the lifetime of the electron−hole pair. Generated electrons in α-Ag_2WO_4 are transferred to AgNPs metal and the electron accumulation increases the Ag negative potential of Ag, which results in an upward shift of the resultant Fermi level (E_f) to the CB of α-Ag_2WO_4. This negative shift in E_f facilitates a better charge separation and more reductive power for the system, which indicates it is very likely that the junction of the system hinders the electron−hole recombination process; thus this improved bactericide activity can be achieved on the Ag/α-Ag_2WO_4 junction.

The overall process and charge transfer mechanism is illustrated in Figure 8 to explain the antimicrobacterial effect. A

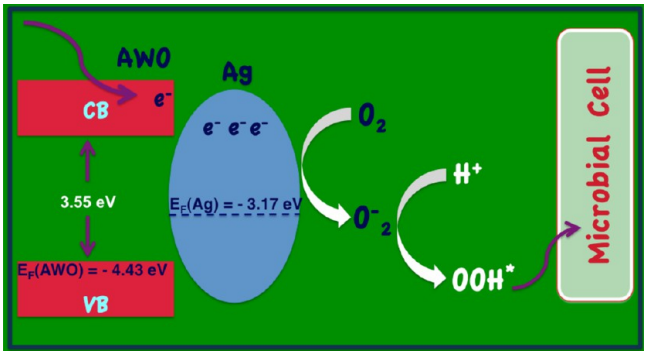

Figure 8. Proposed antimicrobacterial activity mechanism based on the energy band structure and electron−hole pair transfer and separation in α-Ag_2WO_4 with metallic Ag.

discontinuity of e′ and h$^\bullet$ are formed in the α-Ag_2WO_4 and metallic Ag at short-range because the metallic Ag was reduced and emerged from the α-Ag_2WO_4 surface as discussed in HRTEM results ($Ag^+ + 1e^- \rightarrow Ag^0$). This fact creates a disorder in the α-Ag_2WO_4 semiconductor and the formation of e′ and h$^\bullet$ pairs. Our group[1,7,80] previously discussed the formation of e′ and h$^\bullet$ in bulk and surface of tungstates with a scheelite structure (AWO_4, where A = Ca, Sr, Ba) via formation of complex clusters ($[WO_3{\cdot}V_O^z]^{81-83}$ and $[AO_7{\cdot}V_O^z]^{83}$ (where $V_O^z = V_O^x, V_O^\bullet, V_O^{\bullet\bullet}$) as derived from structural disorders.

As observed in the DOS diagram (Figure 6), metallic Ag is formed by delocalized electrons; in our case, AgNPs extend the lifetime of the electron−hole pair formed in the semiconductor to the microbial solution. Ag nanofilaments formed from the α-Ag_2WO_4 crystal surface increase, and they are capable of enhancing the charge transfer process to the solution and producing a 4-fold the bactericidal effect increase.

Thus, the interaction between the semiconductor and the Ag^0 metallic promotes trapping and conduction of e′ and h$^\bullet$ pairs without light-induced radiation. In a second step, the Ag^0 and α-Ag_2WO_4 surface interact with H_2O or/and O_2 depending on the chemical environment. Generated OH* and HO_2^* radicals will indiscriminately attack cell wall polysaccharides, membrane lipids, and membrane proteins whose integrity is critical for cellular survival. The abundance and peripheral location of the cell envelope polysaccharides mark them as the first target, and only after this barrier has been breached can the highly reactive radicals directly attack the cell membrane, whose integrity is critical for cellular survival. The cell membrane not only is the ultimate barrier between the environment and the cell interior but also is critical for the function of membrane-associated proteins.[84] Possibly a small amount of the metallic Ag surface undergoes oxidation at the interface with the aqueous solution. Then Ag^+ ions migrate from the nanoparticle surface toward the solution. Generally, AgNPs and Ag^+ ions have a high affinity to react with sulfur- and phosphorus-containing compounds inside or outside the cell membrane, which in turn affects bacterial cell viability.[15]

Thus, results of this investigation indicate that synthesized α-Ag_2WO_4 holds great promise as an alternative to the antibiotic of last resort, vancomycin: bacteria have already started to develop a resistance to vancomycin. Also, for the first time, our results demonstrate that irradiation by an electron beam from the electronic microscope enhances the antimicrobial effect of the α-Ag_2WO_4 solution and thus reduces the minimum nanoparticle concentration required to kill MRSA.

Finally, note that the performance of nanosilver as an antimicrobacterial agent after its initial employment has not been investigated and therefore prompts further research. Indeed, this investigation may help engineer nanosilver products that retain their antibacterial activity mostly by the nanosilver contact, which is essential before nanosilver is used for specialized treatments in hospitals, as fillers in textiles, as polymers for biomedical uses (e.g., catheters, or in consumer products for everyday use.

5. CONCLUSIONS

In this study, a α-Ag_2WO_4 orthorhombic phase was successfully obtained by using the MH method (AWO). The α-Ag_2WO_4 surface was irradiated by electron bean irradiation, which

dx.doi.org/10.1021/jp410564p | J. Phys. Chem. A XXXX, XXX, XXX−XXX

promoted Ag metallic nanofilament growth (AWO:Ag). These samples were characterized by XRD, FT-Raman spectroscopy, and UV−vis measurements as well as electron microscopy (FE-SEM, TEM, and HRTEM) where an electron beam was used for structural and morphological characterization. In addition, a framework is proposed for understanding the antimicrobacterial effect to combat planktonic cells of methicillin-resistant *S. aureus* (MRSA) of both samples, which is based on the analysis of the results obtained by experimental techniques and first-principle calculations.

The main conclusions can be summarized as follows: (i) Structural analysis of XRD reveals that at long-range, both AWO and AWO:Ag samples are ordered whereas Raman analysis renders a broadening spectra that indicates a structural disorder at short-range. (ii) STEM images underscore the absence of an interface between the α-Ag_2WO_4 matrix and Ag nanofilament growth. This feature provides special and unique properties for this new material, which is not a core−shell, a decorated structure, or even a heterostructure, and is therefore a continuous structure composed of a semiconductor and a metal. (iii) The electron beam provokes a structural and electronic disorder on this material that modifies $[WO_6]$ and $[AgO_y]_{y=7,6,4,2}$ cluster constituents and the formation of metallic Ag. (iv) A 4-fold enhancement of the antimicrobacterial effect was observed in the α-Ag_2WO_4\Ag junction of the AWO:Ag sample. (v) Experimental data and theoretical calculations suggest that this enhancement originates from the coupling between α-Ag_2WO_4 and Ag and promotes electron and hole transfer processes that can readily participate in antimicrobacterial processes. From an electronic perspective, this activity can be closely related to the energy level alignment: VBs and CBs of α-Ag_2WO_4 and Ag are well positioned (energetically); i.e., the activated Ag can act as an electron trap or as a sink of generated electrons that aids electron−hole separation and induces a local electromagnetic field capable of easing the electron excitation. This result corresponds to the coupling in a plasmonic system that can be visualized in terms of either electric or magnetic near fields; i.e., surface plasmon induced localized heating of AgNPs can produce the chemical degradation of MRSA on the AgNPs. (vi) The surface of Ag and α-Ag_2WO_4 interacts with H_2O or/and O_2 depending on the chemical environment generating OH* and HO_2^* radicals that will indiscriminately attack cell wall polysaccharides, membrane, and membrane proteins whose integrity is critical for cellular survival.

The creation of new materials has always been fascinating to researchers as it provides immense opportunities to study the emergence of novel physical and chemical properties. Quite often newly identified materials facilitate the discovery of novel phenomena. One such example, which can change the directions of noble metal research is the production of AgNPs by irradiation of α-Ag_2WO_4 microcrystals by employing an electron beam. Results of this research provide fundamental insight into the role of a junction in antimicrobacterial activity. From a practical point of view, we believe that the combination of α-Ag_2WO_4 and AgNPs not only has outstanding potential in biological applications but also shows potential promise for applications in sensors, solar cells, catalysis, separation technology, etc. These studies are currently in progress.

■ ASSOCIATED CONTENT

Supporting Information

XRD patterns and spectral dependence of the absorbance. This information is available free of charge via the Internet at http://pubs.acs.org

■ AUTHOR INFORMATION

Corresponding Author

*V. M. Longo: e-mail, valerialongo@liec.ufscar.br; phone, +55-16-3373-9828.

Notes

The authors declare no competing financial interest.

■ ACKNOWLEDGMENTS

The authors are thankful for the financial support of the Brazilian research financing institutions: CAPES, CNPq (151136-2013-0, 350711-2012-7), and FAPESP and LME/LNNano/CNPEM where the transmission electron microscopy analyses were developed. J. Andrés also acknowledges Generalitat Valenciana for the Prometeo/2009/053 project, Ministerio de Ciencia e Innovación for project CTQ2009-14541-C02, and Programa de Cooperación Científica con Iberoamerica (Brasil), Ministerio de Educación (PHB2009-0065-PC).

■ REFERENCES

(1) Longo, V. M.; Gracia, L.; Stroppa, D. G.; Cavalcante, L. S.; Orlandi, M.; Ramirez, A. J.; Leite, E. R.; Andres, J.; Beltran, A.; Varela, J. A.; et al. A Joint Experimental and Theoretical Study on the Nanomorphology of CaWO4 Nanocrystals. *J. Phys. Chem. C* **2011**, *115*, 20113−20119.

(2) Muller-Buschbaum, H. On The Crystal Chemistry Of Oxoargentates And Silveroxometallates. *Z. Anorg. Allg. Chem.* **2004**, *630*, 2125−2175.

(3) Vandenberg, A. J.; Juffermans, C. A. H. The Polymorphism of Silver Tungstate Ag-2Wo4. *J. Appl. Crystallogr.* **1982**, *15*, 114−116.

(4) Skarstad, P. M.; Geller, S. (W4O16)8- Polyion in High-Temperature Modification Of Silver Tungstate. *Mater. Res. Bull.* **1975**, *10*, 791−799.

(5) Phuruangrat, A.; Thongtem, T.; Thongtem, S. Synthesis of Lead Molybdate And Lead Tungstate Via Microwave Irradiation Method. *J. Cryst. Growth* **2009**, *311*, 4076−4081.

(6) Phuruangrat, A.; Thongtem, T.; Thongtem, S. Barium Molybdate And Barium Tungstate Nanocrystals Synthesized By A Cyclic Microwave Irradiation. *J. Phys. Chem. Solids* **2009**, *70*, 955−959.

(7) Gracia, L.; Longo, V. M.; Cavalcante, L. S.; Beltran, A.; Avansi, W.; Li, M. S.; Mastelaro, V. R.; Varela, J. A.; Longo, E.; Andres, J. Presence Of Excited Electronic State In Cawo(4) Crystals Provoked By A Tetrahedral Distortion: An Experimental And Theoretical Investigation. *J. Appl. Phys.* **2011**, *110*, 043501−043511.

(8) Raubach, C. W.; de Santana, Y. V. B.; Ferrer, M. M.; Longo, V. M.; Varela, J. A.; Avansi, W.; Buzolin, P. G. C.; Sambrano, J. R.; Longo, E. Strutural and Optical Approach Of Cds@Zns Core-Shell System. *Chem. Phys. Lett.* **2012**, *536*, 96−99.

(9) Mera, R. M.; Suaya, J. A.; Amrine-Madsen, H.; Hogea, C. S.; Miller, L. A.; Lu, E. P.; Sahm, D. F.; O'Hara, P.; Acosta, C. J. Increasing Role of Staphylococcus Aureus And Community-Acquired Methicillin-Resistant Staphylococcus Aureus Infections in the United States: A 10-Year Trend of Replacement and Expansion. *Microb. Drug Resist.* **2011**, *17*, 321−328.

(10) Cosgrove, S. E.; Sakoulas, G.; Perencevich, E. N.; Schwaber, M. J.; Karchmer, A. W.; Carmeli, Y. Comparison of Mortality Associated With Methicillin-Resistant And Methicillin-Susceptible Staphylococcus Aureus Bacteremia: A Meta-Analysis. *Clin. Infect. Dis.* **2003**, *36*, 53−59.

(11) Nickerson, E. K.; Hongsuwan, M.; Limmathurotsakul, D.; Wuthiekanun, V.; Shah, K. R.; Srisomang, P.; Mahavanakul, W.; Wacharaprechasgul, T.; Fowler, V. G.; West, T. E.; et al. Staphylococcus

aureus Bacteraemia in a Tropical Setting: Patient Outcome and Impact of Antibiotic Resistance. *PLoS One* **2009**, *4*, 1−7.
(12) van Hal, S. J.; Jensen, S. O.; Vaska, V. L.; Espedido, B. A.; Paterson, D. L.; Gosbell, I. B. Predictors of Mortality in Staphylococcus aureus Bacteremia. *Clin. Microbiol. Rev.* **2012**, *25*, 362−386.
(13) Stevens, D. L. The role of Vancomycin In The Treatment Paradigm. *Clin. Infect. Dis.* **2006**, *42*, S51−S57.
(14) Sakoulas, G.; Moise-Broder, P. A.; Schentag, J.; Forrest, A.; Moellering, R. C.; Eliopoulos, G. M. Relationship Of MIC And Bactericidal Activity To Efficacy Of Vancomycin For Treatment Of Methicillin-Resistant Staphylococcus Aureus Bacteremia. *J. Clin. Microbiol.* **2004**, *42*, 2398−2402.
(15) Morones, J. R.; Elechiguerra, J. L.; Camacho, A.; Holt, K.; Kouri, J. B.; Ramirez, J. T.; Yacaman, M. J. The Bactericidal Effect Of Silver Nanoparticles. *Nanotechnology* **2005**, *16*, 2346−2353.
(16) Kim, J. S.; Kuk, E.; Yu, K. N.; Kim, J. H.; Park, S. J.; Lee, H. J.; Kim, S. H.; Park, Y. K.; Park, Y. H.; Hwang, C. Y.; et al. Antimicrobial Effects Of Silver Nanoparticles. *Nanomed.-Nanotechnol. Biol. Med.* **2007**, *3*, 95−101.
(17) Rai, M.; Yadav, A.; Gade, A. Silver Nanoparticles As A New Generation Of Antimicrobials. *Biotechnol. Adv.* **2009**, *27*, 76−83.
(18) Liao, H. W.; Nehl, C. L.; Hafner, J. H. Biomedical Applications Of Plasmon Resonant Metal Nanoparticles. *Nanomedicine* **2006**, *1*, 201−208.
(19) http://www.nanotechproject.org/inventories/.
(20) Bhattacharyya, S.; Kudgus, R. A.; Bhattacharya, R.; Mukherjee, P. Inorganic Nanoparticles in Cancer Therapy. *Pharm. Res.* **2011**, *28*, 237−259.
(21) Yildirimer, L.; Thanh, N. T. K.; Loizidou, M.; Seifalian, A. M. Toxicological Considerations Of Clinically Applicable Nanoparticles. *Nano Today* **2011**, *6*, 585−607.
(22) Eckhardt, S.; Brunetto, P. S.; Gagnon, J.; Priebe, M.; Giese, B.; Fromm, K. M. Nanobio Silver: Its Interactions with Peptides and Bacteria, and Its Uses in Medicine. *Chem. Rev.* **2013**, *113*, 4708−4754.
(23) Chernousova, S.; Epple, M. Silver as Antibacterial Agent: Ion, Nanoparticle, and Metal. *Angew. Chem. Int. Ed.* **2013**, *52*, 1636−1653.
(24) Lok, C. N.; Ho, C. M.; Chen, R.; He, Q. Y.; Yu, W. Y.; Sun, H. Z.; Tam, P. K. H.; Chiu, J. F.; Che, C. M. Proteomic Analysis Of The Mode Of Antibacterial Action Of Silver Nanoparticles. *J. Proteome Res.* **2006**, *5*, 916−924.
(25) Sotiriou, G. A.; Teleki, A.; Camenzind, A.; Krumeich, F.; Meyer, A.; Panke, S.; Pratsinis, S. E. Nanosilver On Nanostructured Silica: Antibacterial Activity And Ag Surface Area. *Chem. Eng. J.* **2011**, *170*, 547−554.
(26) Pal, S.; Tak, Y. K.; Song, J. M. Does The Antibacterial Activity Of Silver Nanoparticles Depend On The Shape Of The Nanoparticle? A Study Of The Gram-Negative Bacterium Escherichia Coli. *Appl. Environ. Microbiol.* **2007**, *73*, 1712−1720.
(27) Murugan, E.; Vimala, G. Effective Functionalization Of Multiwalled Carbon Nanotube With Amphiphilic Poly-(Propyleneimine) Dendrimer Carrying Silver Nanoparticles For Better Dispersability And Antimicrobial Activity. *J. Colloid Interface Sci.* **2011**, *357*, 354−365.
(28) Feng, Q. L.; Wu, J.; Chen, G. Q.; Cui, F. Z.; Kim, T. N.; Kim, J. O. A Mechanistic Study Of The Antibacterial Effect Of Silver Ions On Escherichia Coli And Staphylococcus Aureus. *J. Biomed. Mater. Res.* **2000**, *52*, 662−668.
(29) Panacek, A.; Kvitek, L.; Prucek, R.; Kolar, M.; Vecerova, R.; Pizurova, N.; Sharma, V. K.; Nevecna, T.; Zboril, R. Silver Colloid Nanoparticles: Synthesis, Characterization, And Their Antibacterial Activity. *J. Phys. Chem. B* **2006**, *110*, 16248−16253.
(30) Ruparelia, J. P.; Chatterjee, A. K.; Duttagupta, S. P.; Mukherji, S. Strain Specificity In Antimicrobial Activity Of Silver And Copper Nanoparticles. *Acta Biomater.* **2008**, *4*, 707−716.
(31) Choi, O.; Hu, Z. Q. Size Dependent And Reactive Oxygen Species Related Nanosilver Toxicity To Nitrifying Bacteria. *Environ. Sci. Technol.* **2008**, *42*, 4583−4588.
(32) Miao, A. J.; Schwehr, K. A.; Xu, C.; Zhang, S. J.; Luo, Z. P.; Quigg, A.; Santschi, P. H. The Algal Toxicity Of Silver Engineered Nanoparticles And Detoxification By Exopolymeric Substances. *Environ. Pollut.* **2009**, *157*, 3034−3041.
(33) Hook, S. E.; Fisher, N. S. Sublethal Effects Of Silver In Zooplankton: Importance Of Exposure Pathways And Implications For Toxicity Testing. *Environ. Toxicol. Chem.* **2001**, *20*, 568−574.
(34) Laban, G.; Nies, L. F.; Turco, R. F.; Bickham, J. W.; Sepulveda, M. S. The Effects Of Silver Nanoparticles On Fathead Minnow (Pimephales Promelas) Embryos. *Ecotoxicology* **2010**, *19*, 185−195.
(35) Kim, J. H.; Lee, S. M.; Jun, B. H.; Choi, H. J.; Kim, J. S.; Cho, M. H.; Kim, Y. K.; Jeong, D. H.; Lee, Y. S. Multiplex Detection And Imaging Of Cancer Markers Based On Surface-Enhanced Raman Spectroscopic Nanoparticle Probes (SERS Dots). *Nanomed.-Nanotechnol. Biol. Med.* **2007**, *3*, 341−341.
(36) Cui, X. Q.; Li, C. M.; Bao, H. F.; Zheng, X. T.; Lu, Z. S. In Situ Fabrication Of Silver Nanoarrays In Hyaluronan/PDDA Layer-By-Layer Assembled Structure. *J. Colloid Interface Sci.* **2008**, *327*, 459−465.
(37) Daallas, P.; Sharma, V. K.; Zboril, R. Silver Polymeric Nanocomposites As Advanced Antimicrobial Agents: Classification, Synthetic Paths, Applications, And Perspectives. *Adv. Colloid Interface Sci.* **2011**, *166*, 119−135.
(38) Gravante, G.; Caruso, R.; Sorge, R.; Nicoli, F.; Gentile, P.; Cervelli, V. Nanocrystalline Silver A Systematic Review of Randomized Trials Conducted on Burned Patients and an Evidence-Based Assessment of Potential Advantages Over Older Silver Formulations. *Ann. Plast. Surg.* **2009**, *63*, 201−205.
(39) Tian, J.; Wong, K. K. Y.; Ho, C. M.; Lok, C. N.; Yu, W. Y.; Che, C. M.; Chiu, J. F.; Tam, P. K. H. Topical Delivery Of Silver Nanoparticles Promotes Wound Healing. *ChemMedChem* **2007**, *2*, 129−136.
(40) Madhumathi, K.; Kumar, P. T. S.; Abhilash, S.; Sreeja, V.; Tamura, H.; Manzoor, K.; Nair, S. V.; Jayakumar, R. Development of Novel Chitin/Nanosilver Composite Scaffolds For Wound Dressing Applications. *J. Mater. Sci.-Mater. Med.* **2010**, *21*, 807−813.
(41) Lackner, P.; Beer, R.; Broessner, G.; Helbok, R.; Galiano, K.; Pleifer, C.; Pfausler, B.; Brenneis, C.; Huck, C.; Engelhardt, K.; et al. Efficacy Of Silver Nanoparticles-Impregnated External Ventricular Drain Catheters In Patients With Acute Occlusive Hydrocephalus. *Neurocrit. Care* **2008**, *8*, 360−365.
(42) Chaloupka, K.; Malam, Y.; Seifalian, A. M. Nanosilver As A New Generation Of Nanoproduct In Biomedical Applications. *Trends Biotechnol.* **2010**, *28*, 580−588.
(43) Magana, S. M.; Quintana, P.; Aguilar, D. H.; Toledo, J. A.; Angeles-Chavez, C.; Cortes, M. A.; Leon, L.; Freile-Pelegrin, Y.; Lopez, T.; Sanchez, R. M. T. Antibacterial Activity Of Montmorillonites Modified With Silver. *J. Mol. Catal. A-Chem.* **2008**, *281*, 192−199.
(44) Joya, Y. F.; Liu, Z.; Wang, T. Characterization And Antibacterial Functions Of Ag-Tio2 And W-Tio2 Nanostructured Thin Films Prepared By Sol-Gel/Laser-Induced Technique. *Appl. Phys. B-Lasers Opt* **2011**, *105*, 525−536.
(45) Height, M. J.; Pratsinis, S. E. Antimicrobial and Antifungal Powders Made by Flame Spray Pyrolysis. European Patent 2007, EP1846327 (A1846321).
(46) Kong, H.; Jang, J. Antibacterial Properties Of Novel Poly(Methyl Methacrylate) Nanofiber Containing Silver Nanoparticles. *Langmuir* **2008**, *24*, 2051−2056.
(47) Loher, S.; Schneider, O. D.; Maienfisch, T.; Bokorny, S.; Stark, W. J. Micro-organism-triggered Release Of Silver Nanoparticles From Biodegradable Oxide Carriers Allows Preparation Of Self-Sterilizing Polymer Surfaces. *Small* **2008**, *4*, 824−832.
(48) Kumar, R.; Munstedt, H. Silver Ion Release From Antimicrobial Polyamide/Silver Composites. *Biomaterials* **2005**, *26*, 2081−2088.
(49) Schiffman, J. D.; Wang, Y.; Giannelis, E. P.; Elimelech, M. Biocidal Activity of Plasma Modified Electrospun Polysulfone Mats Functionalized with Polyethyleneimine-Capped Silver Nanoparticles. *Langmuir* **2011**, *27*, 13159−13164.
(50) Kumar, A.; Vemula, P. K.; Ajayan, P. M.; John, G. Silver-Nanoparticle-Embedded Antimicrobial Paints Based On Vegetable Oil. *Nat. Mater.* **2008**, *7*, 236−241.

(51) Liu, J. Y.; Sonshine, D. A.; Shervani, S.; Hurt, R. H. Controlled Release of Biologically Active Silver from Nanosilver Surfaces. *ACS Nano* **2010**, *4*, 6903−6913.
(52) Li, W. R.; Xie, X. B.; Shi, Q. S.; Zeng, H. Y.; Ou-Yang, Y. S.; Chen, Y. B. Antibacterial Activity And Mechanism Of Silver Nanoparticles On Escherichia Coli. *Appl. Microbiol. Biotechnol.* **2010**, *85*, 1115−1122.
(53) Knetsch, M. L. W.; Koole, L. H. New Strategies in the Development of Antimicrobial Coatings: The Example of Increasing Usage of Silver and Silver Nanoparticles. *Polymers* **2011**, *3*, 340−366.
(54) Dal Lago, V.; de Oliveira, L. F.; Goncalves, K. D.; Kobarg, J.; Cardoso, M. B. Size-selective Silver Nanoparticles: Future Of Biomedical Devices With Enhanced Bactericidal Properties. *J. Mater. Chem.* **2011**, *21*, 12267−12273.
(55) Levinson, W. *Review of Medical Microbiology and Immunology*; McGraw-Hill Professional: New York, 2006.
(56) Fayaz, A. M.; Balaji, K.; Girilal, M.; Yadav, R.; Kalaichelvan, P. T.; Venketesan, R. Biogenic Synthesis Of Silver Nanoparticles And Their Synergistic Effect With Antibiotics: A Study Against Gram-Positive And Gram-Negative Bacteria. *Nanomed.-Nanotechnol. Biol. Med.* **2010**, *6*, 103−109.
(57) Cavalcante, L. S.; Almeida, M. A. P.; Avansi, W.; Tranquilin, R. L.; Longo, E.; Batista, N. C.; Mastelaro, V. R.; Li, M. S. Cluster Coordination and Photoluminescence Properties of alpha-Ag2WO4-Microcrystals. *Inorg. Chem.* **2012**, *51*, 10675−10687.
(58) Longo, E.; Cavalcante, L. S.; Volanti, D. P.; Gouveia, A. F.; Longo, V. M.; Varela, J. A.; Orlandi, M. O.; Andrés, J. Direct In Situ Observation Of The Electron-Driven Synthesis Of Ag Filaments On A-Ag2WO4 Crystals. *Sci. Rep* **2013**, *3*, 1676.
(59) Longo, E.; Cavalcante, L. S.; Volanti, D. P.; Longo, V. M.; Gracia, L.; Nogueira, I. C.; Almeida, M. A. P.; Ferrer, M. M.; Andrés, J. Toward an Understanding of the Growth of Ag Filaments on α-Ag2WO4 and their Photoluminescent Properties: A Combined Experimental and Theoretical Study. *J. Chem. Phys. C* **2014**, *118*, 1229−1239.
(60) Dovesi, R.; Saunders, V. R.; Roetti, C.; Orlando, R.; Zicovich-Wilson, C. M.; Pascale, F.; Civalleri, B.; Doll, K.; Harrison, N. M.; Bush, I. J.; et al. *CRYSTAL09 User's Manual*; University of Torino: Torino, 2009.
(61) Becke, A. D. Density-Functional Thermochemistry 0.3. the Role of Exact Exchange. *J. Chem. Phys.* **1993**, *98*, 5648−5652.
(62) Lee, C. T.; Yang, W. T.; Parr, R. G. Development of the Colle-Salvetti Correlation-Energy Formula into a Functional of the Electron-Density. *Phys. Rev. B* **1988**, *37*, 785−789.
(63) Corà, F.; Alfredsson, M.; Mallia, G.; Middlemiss, D. S.; Mackrodt, W.; Dovesi, R.; Orlando, R. *Struct. Bonding (Berlin)*; Springer-Verlag: Berlin, 2004.
(64) Monkhorst, H. J.; Pack, J. D. Special Points for Brillouin-zone Integrations. *Phys. Rev. B* **1976**, *13*, 5188−5192.
(65) http://www.crystal.unito.it/Basis_Sets/Ptable.html.
(66) Kokalj, A. XCrySDen - A New Program For Displaying Crystalline Structures And Electron Densities. *J. Mol. Graph.* **1999**, *17*, 176.
(67) Tsuji, M.; Gomi, S.; Maeda, Y.; Matsunaga, M.; Hikino, S.; Uto, K.; Tsuji, T.; Kawazumi, H. Rapid Transformation from Spherical Nanoparticles, Nanorods, Cubes, or Bipyramids to Triangular Prisms of Silver with PVP, Citrate, and H2O2. *Langmuir* **2012**, *28*, 8845−8861.
(68) Yasuda, K.; Hirano, Y.; Kamino, T.; Yaguchi, T.; Hirokawa, K. Observation Of Vaporization In Palladium-Indium Intermetallic Compounds By Graphite-Furnace Atomic-Absorption Spectrometry Using Transmission Electron-Microscopy. *Anal. Sci.* **1995**, *11*, 437−440.
(69) Wang, P.; Huang, B. B.; Qin, X. Y.; Zhang, X. Y.; Dai, Y.; Whangbo, M. H. Ag/AgBr/WO3 center dot H2O: Visible-Light Photocatalyst for Bacteria Destruction. *Inorg. Chem* **2009**, *48*, 10697−10702.
(70) Turkovic, A.; Fox, D. L.; Scott, J. F.; Geller, S.; Ruse, G. F. High-Temperature Raman-Spectroscopy Of Silver Tetra-Tungstate, Ag8w4o16. *Mater. Res. Bull.* **1977**, *12*, 189−195.
(71) Sczancoski, J. C.; Cavalcante, L. S.; Joya, M. R.; Varela, J. A.; Pizani, P. S.; Longo, E. SrMoO4 Powders Processed In Microwave-Hydrothermal: Synthesis, Characterization And Optical Properties. *Chem. Eng. J.* **2008**, *140*, 632−637.
(72) Wood, D. L.; Tauc, J. Weak Absorption Tails in Amorphous Semiconductors. *Phys. Rev. B* **1972**, *5*, 3144−3151.
(73) Matsumura, Y.; Yoshikata, K.; Kunisaki, S.; Tsuchido, T. Mode of Bactericidal Action Of Silver Zeolite And Its Comparison With That Of Silver Nitrate. *Appl. Environ. Microbiol.* **2003**, *69*, 4278−4281.
(74) Li, W. R.; Xie, X. B.; Shi, Q. S.; Duan, S. S.; Ouyang, Y. S.; Chen, Y. B. Antibacterial Effect Of Silver Nanoparticles On Staphylococcus Aureus. *Biometals* **2011**, *24*, 135−141.
(75) AshaRani, P. V.; Mun, G. L. K.; Hande, M. P.; Valiyaveettil, S. Cytotoxicity and Genotoxicity of Silver Nanoparticles in Human Cells. *ACS Nano* **2009**, *3*, 279−290.
(76) Cabiscol, E.; Tamarit, J.; Ros, J. Oxidative Stress In Bacteria And Protein Damage By Reactive Oxygen Species. *Int. Microbiol.* **2000**, *3*, 3−8.
(77) El-Sayed, M. A. Some Interesting Properties Of Metals Confined In Time And Nanometer Space Of Different Shapes. *Acc. Chem. Res.* **2001**, *34*, 257−264.
(78) Jain, P. K.; Huang, X. H.; El-Sayed, I. H.; El-Sayed, M. A. Noble Metals on the Nanoscale: Optical and Photothermal Properties and Some Applications in Imaging, Sensing, Biology, and Medicine. *Acc. Chem. Res.* **2008**, *41*, 1578−1586.
(79) Scaiano, J. C.; Stamplecoskie, K. Can Surface Plasmon Fields Provide a New Way to Photosensitize Organic Photoreactions? From Designer Nanoparticles to Custom Applications. *J. Phys. Chem. Lett.* **2013**, *4*, 1177−1187.
(80) Cavalcante, L. S.; Longo, V. M.; Sczancoski, J. C.; Almeida, M. A. P.; Batista, A. A.; Varela, J. A.; Orlandi, M. O.; Longo, E.; Li, M. S. Electronic Structure, Growth Mechanism And Photoluminescence Of Cawo4 Crystals. *Crystengcomm* **2012**, *14*, 853−868.
(81) Liu, T. Y.; Chen, J.; Yan, F. N. Optical Polarized Properties Related To The Oxygen Vacancy In The Camoo4 Crystal. *J. Lumin.* **2009**, *129*, 101−104.
(82) Pu, C. Y.; Liu, T. Y.; Zhang, Q. R. Study Of The Electronic Structures Of Camoo4 Crystal Related To Oxygen Vacancy. *Phys. Status Solidi B-Basic Solid State Phys.* **2008**, *245*, 1586−1589.
(83) Longo, V. M.; de Figueiredo, A. T.; Campos, A. B.; Espinosa, J. W. M.; Hernandes, A. C.; Taft, C. A.; Sambrano, J. R.; Varela, J. A.; Longo, E. Different Origins Of Green-Light Photoluminescence Emission In Structurally Ordered And Disordered Powders Of Calcium Molybdate. *J. Phys. Chem. A* **2008**, *112*, 8920−8928.
(84) Stark, G. Functional Consequences Of Oxidative Membrane Damage. *J. Membr. Biol.* **2005**, *205*, 1−16.